MULTIPHYSICS SIMULATION OF RESISTANCE SPOT WELDING

I. BEN BAHAFFA*, **, M. COURTOIS*, S. CADIOU*, E. GESLAIN*, E. COURTOIS*, T. DUPUY**, X. CHEN**

** Univ. Bretagne Sud, UMR CNRS 6027, IRDL, F-56100 Lorient, France*
*** ArcelorMittal – Global Research and Development Maizières Products, F-57280 Maizières-lès-Metz, France*

DOI 10.3217/978-3-99161-089-2-017, license CC BY 4.0

ABSTRACT

Resistance spot welding is widely used in the automotive industry for assembling steel car bodies. However, increasing demands for safety, durability, and weight reduction have led to the development of more advanced steels, which are also more sensitive to welding defects. To better understand issues like material expulsion, this study relies on an innovative multiphysics finite element numerical simulation.

The developed model integrates all the main physical phenomena involved in the process: heat transfer, fluid flow, electromagnetism, and solid mechanics. To manage this complexity, a multi-mesh approach is used, allowing each physics to be solved on a dedicated mesh while maintaining efficient coupling at each time step. The results of this new method will be compared with a more classical Electro-Thermo-Mechanical model, which is the industry standard to highlight the advantages of our approach for studying interfacial expulsion.

Keywords: resistance spot welding, expulsion, numerical simulation, multi-physics coupling, CFD

INTRODUCTION

The most used welding method in the automotive industry is resistance spot welding (RSW), a joining technique that involves the local melting of materials by Joule heating between two or three sheets. However, new challenges have emerged regarding the weldability of some newly developed steels. In fact, modern ultra-high-strength steels sometimes have a more restricted weldability range due to several unwanted phenomena, including expulsion.

Expulsion is a defect where the molten material between the sheets is violently expelled during welding process. This phenomenon can seriously degrade the mechanical properties of the weld nugget and generates a safety hazard to people and machines around production lines. The molten nugget is usually contained by the electrode pressing on the weld, but as the thermal expansion increases so do the internal pressure of the nugget, which may cause the

expulsion if the containment is insufficient [1]. This reduces the size of the weld and its mechanical strength, making it non-compliant. Expulsion mainly occurs at the sheet interface and typically defines the maximum welding current. The minimum current ensures a sufficient weld diameter, and the range between this minimum and the expulsion limit defines the welding range (NF EN ISO 18278-2, SEP1220-2). Excessive current causes expulsion, although it is not systematic and occurs unpredictably.

Since the 1990s, numerical simulation has improved our understanding of welding phenomena. Electro-thermo-mechanical-metallurgical (ETMM) models can predict the mechanical behavior of the weld nugget, but not expulsion, as they neglect fluid flow and magnetic fields. However, these physics are needed to calculate flow behavior within the molten pool, which modifies heat transfer distribution and equalizes temperature in the nugget ([2];[3]). A magneto-hydrodynamic model [4] shows that convection can reach 0.5 m/s, and the resulting temperature is lower than that predicted by ETMM models. Therefore, an effective simulation of expulsion requires a model that integrates electromagnetism, fluid flow, and solid mechanics.

To our knowledge, such a fully coupled multiphysics model does not yet exist in the literature to provide a better understanding of expulsion onset. However, some studies specifically aim to predict this phenomenon. Browne et al. [5] proposed a criterion based on the ratio between the molten nugget radius (Rn) and the compressive contact radius (Rcontact), explaining how increased electrode clamping force delays expulsion. This criterion was reused by Zhang, Shen, & Lai [6]. Senkara et al. [1] and Valaee-Tale [7] describe a “force balance model”, comparing the effective force of the electrodes to the pressure inside the nugget, accounting for liquid compressibility and volume changes. Poor electrode symmetry could also lead to premature expulsion.

In this paper, a new approach of resistance spot welding (RSW) simulation is presented. This method enables the coupling of fluid flow and solid mechanics within the RSW process. A 2D axisymmetric finite element model is proposed, integrating electromagnetic, heat transfer, mechanical, and fluid flow phenomena. The mathematical formulation of the problem is first introduced, followed by a detailed description of the proposed approach. Finally, to demonstrate the potential of this method, a comparison with a classical electro-thermo-mechanical (ETM) model and experimental data is provided.

MATHEMATICAL FORMULATION FOR RSW MULTIPHYSICS MODELING

Since the resistance spot welding process is multiphysic, modelling it involves several strongly coupled physical phenomena, which makes it a complex simulation.

Many phenomena involved are governed by solid mechanics. During welding, the electrodes indent the sheets, creating variable contact between the different components. This contact evolves with temperature, which is itself influenced by the electric current flowing through the assembly. Moreover, the current density passing through the sheets directly depends on the contact area generated by the indentation. These interactions highlight the strong interdependence between electrical, thermal, and mechanical phenomena, which are often modelled using an electro-thermo-mechanical (ETM) approach.

The novelty of our approach lies in the introduction of additional couplings: fluid flow and magnetism. Indeed, during the formation of the molten nugget, a very high pressure can develop, sufficient to slightly push back the electrodes during the welding process. With this addition, our goal is to better represent convection effects in the molten pool, and thus improve the thermal modelling of the nugget, providing a more accurate description of the phenomena related to its expansion during the process.

MATHEMATICAL DESCRIPTION

In this study, we used for this simulation the commercial finite element software, COMSOL Multiphysics®. The physical phenomena considered include electromagnetism, heat transfer, solid mechanics, and fluid flow (with moving meshes). All the material properties used in the model are dependent on the temperature and were provided by ArcelorMittal.

Electrokinetic equations

Under the quasi-steady-state approximation, electrical phenomena can be treated as an electrokinetic problem, for which the current conservation equation is written as (1).

$$div\vec{J} = 0 \tag{1}$$

where J is the current density in [A·m^{-2}].

The flow of electric current through the material leads to the generation of heat by Joule effect (Q_J), which is related to the electric potential (V) and the current density, according to Ohm's law (2), and expressed as (3).

$$\vec{J} = -\sigma_{elec}\,\overrightarrow{grad}\,V \tag{2}$$

$$Q_J = \frac{1}{\sigma}J^2 = \sigma_{elec}\left(\overrightarrow{grad}\,V\right)^2 \tag{3}$$

where Q_J is in [W/m^3] and σ_{elec} is the electrical conductivity in [S·m^{-1}].

Heat Transfer Equations

Heat conduction and advection are governed by the heat equation, which is derived from the principle of energy conservation, and is expressed in transient form by equation (4). This equation accounts for the energy balance within an elementary volume of material, considering the heat generated by the Joule effect and the dissipation by conduction and advection (through v, the fluid velocity).

$$\rho c_p^* \frac{\partial T}{\partial t} + \rho C_p^* v * \nabla T = \vec{\nabla}\left(\lambda\,\vec{\nabla}\,T\right) + Q_J \tag{4}$$

here, ρ is the density in [kg·m^{-3}], λ the thermal conductivity in [W·m^{-1}·K^{-1}], C_p the equivalent specific heat capacity in [J·kg^{-1}·K^{-1}], and Q_J the volumetric heat source term due to the Joule effect in [W·m^{-3}].

In this model, the phase changes of melting and solidification are modelled using the equivalent specific heat capacity method (5).

$$c_p^*(T) = c_p(T) + L_f D_f(T) \tag{5}$$

$$D_f = \frac{1}{\sqrt{\pi(T_{liq}-T_{sol})^2}} exp\left(-\frac{(T-T_f)^2}{(T_{liq}-T_{sol})^2}\right) \tag{6}$$

with C_p the specific heat capacity [J·kg^{-1}·K^{-1}], L_f the enthalpy of phase change of steel [J·kg^{-1}], D_f the fraction of phase transformed (liquidus–solidus) [K^{-1}], and T_{sol}, T_{liq} respectively the solidus and liquidus temperatures.

Mechanical Equations

The large thermal variations observed in the assembly require the use of mechanical behavior laws adapted to wide temperature ranges. In the context of resistance welding, although the temperatures reached could theoretically induce viscous effects, these remain negligible in our studies due to the small deformations observed (around 5% for thin sheets) [8]. Therefore, an elasto-plastic model with isotropic hardening is sufficient to describe the material behaviour. Moreover, the electrodes are modelled with an elastic law, in accordance with experimental observations reported in the literature [9].

The mechanical problem consists in solving the local mechanical equilibrium equation. In this study, inertial forces are assumed negligible, and the mechanical loads are considered to be static.

$$div(\sigma) + f = 0 \tag{7}$$

where σ is the Cauchy stress tensor and f represents the volume force.

Given the size of the system and the deformations involved, the small deformation assumption can be applied. The balance of macroscopic strains ε can thus be written as:

$$\epsilon = \epsilon^e + \epsilon^{th} + \epsilon^p \tag{8}$$

with ϵ^e the elastic strain, ϵ^{th} the thermal strain due to expansion, and ϵ^p the plastic strain. The elastic part is calculated using Hooke's law, which, for an isotropic material, is expressed as follows:

$$\epsilon^e = \frac{1+\nu}{E}\sigma - \frac{\nu}{E} tr(\sigma) I \tag{9}$$

where E is the Young's modulus, ν the Poisson's ratio, and I the second-order identity tensor.

A large part of the deformation is generated by thermal expansion resulting from the heating of the assembly. This strain can be quantified using equation (10).

$$\epsilon_i^{th} = \alpha_i * \Delta T \tag{10}$$

with $\epsilon_i{}^{th}$ the strain due to thermal expansion, α_i the thermal expansion coefficient of the phase [K^{-1}], and ΔT the temperature change.

During the transition from the solid to the liquid state, a sudden drop in density (ρ) can be observed. This results in a sharp increase in the volumetric expansion coefficient (β_i), which in turn leads to a significant variation in the thermal expansion coefficient (α_i). Equation (11) illustrates how the variation of ρ with respect to temperature influences the expansion coefficient α_i:

$$3\alpha_i = -\frac{1}{\rho} * \frac{\Delta\rho}{\Delta T} \tag{11}$$

Consequently, the plasticity criterion $C_{plasticty}$ can be expressed as follows:

$$C_{plasticity} = \sigma_{VM} - R_p - \sigma_y \tag{12}$$

with σ_y the yield strength, R_p the isotropic hardening (14), and σ_{VM} the von Mises equivalent stress, which can be written as follows:

$$\sigma_{VM} = \sqrt{\frac{3}{2}\sigma' : \sigma'} \quad avec\ \sigma' = \sigma - \frac{1}{3}tr(\sigma)I \tag{13}$$

Within the sheets, a Voce law (14) is used to describe the hardening behavior of the material.

$$R_p = \sigma_{sat}\left(1 - e^{-\beta\epsilon_{pe}}\right) \tag{14}$$

where σ_{sat} denotes the saturation value of the isotropic hardening, β is a material parameter controlling the rate of hardening, and ε_{pe} is the equivalent plastic strain.

Fluid flow Equations

The Navier–Stokes equations describe the motion of fluids by accounting for the conservation of momentum (15) and mass (16).

$$\rho\left[\frac{d\vec{v}}{dt} + \vec{v}.\nabla\vec{v}\right] = -\nabla p + \mu\nabla^2\vec{v} + \overrightarrow{f_{HD}} \tag{15}$$

$$\frac{\partial\rho}{\partial \mathrm{t}} + \nabla.(\rho.\vec{v}) = 0 \tag{16}$$

With $\overrightarrow{f_{HD}} = \overrightarrow{F_{flot}} + \overrightarrow{F_{lorentz}}$, the volume force acting on the fluid, which are detailed later. It is assumed that the molten metal behaves as a Newtonian fluid with variable density in a laminar flow regime. To distinguish motion between solid and molten regions, the equivalent viscosity method is used. This method consists in artificially increasing the viscosity in regions where the temperature is below the melting point, thereby preventing fluid movement. Only the liquid zones, where the viscosity remains low, are then able to flow.

Within the molten pool, convective flows can be generated due to the temperature gradient between the edges of the molten zone and its center. These flows can be described by the following equation based on the Boussinesq approximation:

$$\overrightarrow{F_{flot}} = \left[-\rho \cdot \beta \cdot \left(T - T_{fusion}\right) \cdot \vec{g}\right] \tag{17}$$

Due to the high electric current, an electromagnetic force called the Lorentz force is generated. It acts throughout the metal but is strongest where the current density is highest. This electromagnetic force acts on the molten pool and creates movement in the molten zone that is potentially dominant.

$$\overrightarrow{F_{lorentz}} = \vec{j} * \vec{B} \tag{18}$$

$$\overrightarrow{F_{lorentz}} = \begin{cases} -j_z * B_\theta \\ 0 \\ j_r * B_\theta \end{cases} \tag{19}$$

With $\vec{B} = \begin{cases} 0 \\ B_\theta \\ 0 \end{cases}$

MULTI MESH METHOD

One of the main challenges of our approach lies in managing the fluid-structure interaction. During the resistance spot welding process, a force is applied to an assembly of sheets, then a high electric current passes through the assembly, causing the metal to melt at the interface between the sheets. This creates a significant challenge in handling the fluid-solid interface. Indeed, at the beginning of the process, the material is entirely solid, but as welding progresses, it gradually transforms from solid to liquid, thereby creating a moving fluid-structure interface starting from nothing.

To address this, we used the Multi-Mesh method [10]. This approach allows the use of different meshes to solve the same problem, each specifically adapted to the physics it represents. An interpolation and projection method of variables between meshes at each time step then enables the redefinition of all couplings from one mesh to another.

The classical approach generally consists in using a single mesh, constructed according to the constraints of the most restrictive equation. In contrast, here, the use of distinct meshes for each coherent group of equations allows for optimization of local accuracy. However, this decoupling requires projecting solutions between meshes via interpolation, which can lead to a loss of precision, especially when transferring from a fine mesh to a coarser one. Through a process of validation and convergence study not presented here, the model remains relevant, as demonstrated previously [10].

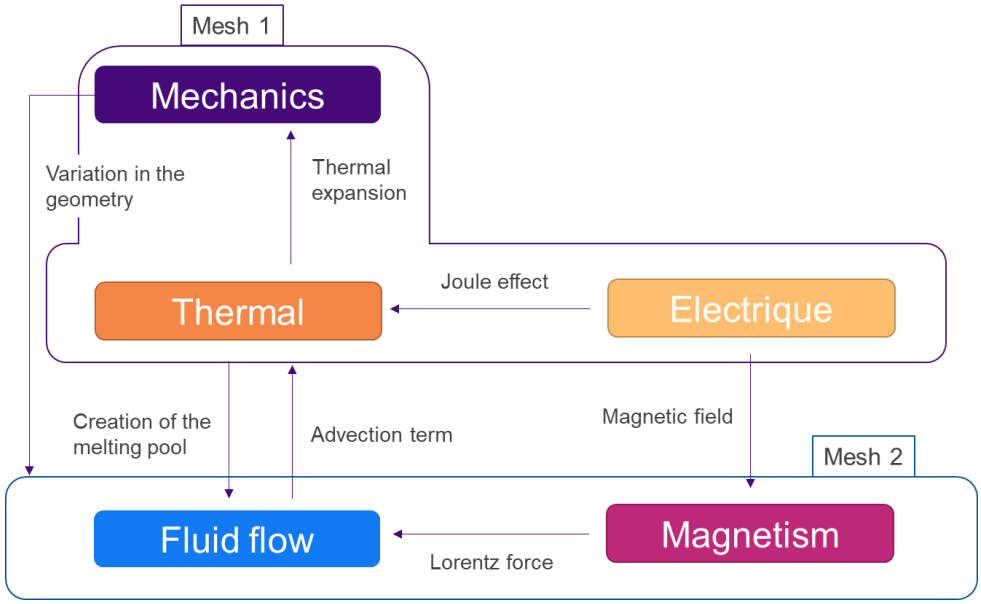

Fig. 1 Diagram of multiphysics couplings and the resolution meshes for each physics

Fig 1 shows the distribution of the physics according to the meshes. In mesh 1, the problems of solid mechanics, heat transfer, and electrical physics are solved. Then, in a second mesh, the fluid flow and magnetism problems are solved. The solution can be considered a strong coupling, as all physics are solved at each time step. In this version of the model, the fluid-structure coupling is done through geometry changes, by imposing the displacement field obtained from solid mechanics onto mesh 2 (where fluid flow is solved), which is modified using an ALE moving mesh method. Thus, fluid flow is solved in the correct deformed geometry, allowing very precise calculation of the thermal field, a central element of the entire problem. The use of two meshes eliminates the issue of the appearance of the liquid zone and simplifies convergence.

Meshes

Using mesh 1, the following physics are solved: solid mechanics, electrical, and heat transfer.

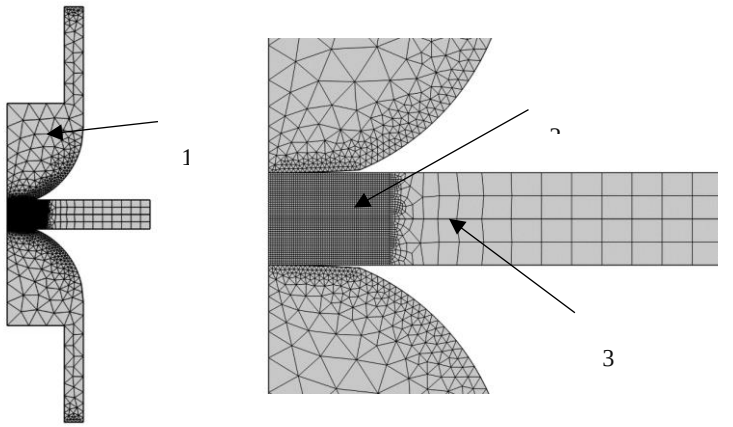

Fig. 2 Distribution of elements in mesh 1

The geometry is divided into three key regions, each meshed according to its importance using triangular or quadrilateral elements:

1. Electrodes (Free triangles, max size: 2.8 mm)
2. Sheets – contact zones between Electrode/Sheet (E/S) and Sheet/Sheet (S/S), as well as the weld nugget development area (Structured quadrilaterals, max size: 0.07 mm)
3. Sheets – area outside the weld nugget (Free quadrilaterals, max size: 1 mm)

Using mesh 2, the following physics are solved: fluid flow and magnetism (for Lorentz forces).

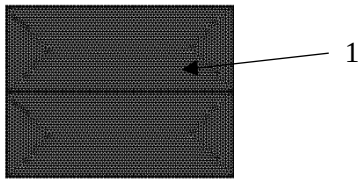

Fig. 3 Distribution of elements in mesh

1. Fusion zone development area. (Free triangles, maximum size 0.06 mm)

RESULTS AND DISCUSSION

WELDING PARAMETERS

The welding parameters are defined by several standards. In our case, we used the SEP-1220-2 standard, which provides welding parameters based on the thickness of the sheet used, the mechanical strength of the steel grade (Rm), and the presence of a coating. Our case describes a symmetrical assembly of DP600 steel sheets with a thickness of 1.5 mm and no coating. Using the material properties of the studied grade, the following welding parameters were chosen (the electrode geometry is described by the ISO 5821 norm):

Table 1 *:* Welding parameters provided by the SEP-1220-2 standard for the steel grade studied

Type of electrodes	Welding force	Numbers of pulses	Welding time	Hold time
F1-16-20-6	4.5 kN	1	340 ms	250 ms

RESULTS AND COMPARISON WITH AN ELECTRO-THERMO-MECHANICAL MODEL

The most commonly used models in the industry are the Electro-Thermo-Mechanical (ETM) numerical models. These models are generally used to predict the size of the molten pool. However, the absence of fluid flow prevents an accurate representation of the temperature field, with calculated temperatures often significantly higher than those observed in reality. To benchmark our model, we compared it to this type of ETM model in order to highlight the possible differences. Thus, two 2D axisymmetric models were solved using the same software, COMSOL Multiphysics 6.2®, and under similar conditions and assumptions. The multiphysics model including fluid flow is referred to as the ETMMHD (Electrical – Thermal – Mechanics – Magnetic – Hydrodynamics).

Fig 4 presents a mirrored view of the 2D axisymmetric model. It illustrates the stress and the displacements along the vertical axis (z axis). One can observe the separation of the sheets caused by indentation, as well as their thermal expansion. A very small displacement is visible at the electrode level, which can be explained by the thermal expansion of the sheet. As the thermal expansion is slightly lifting the electrodes, it’s almost resetting the displacement of the electrodes.

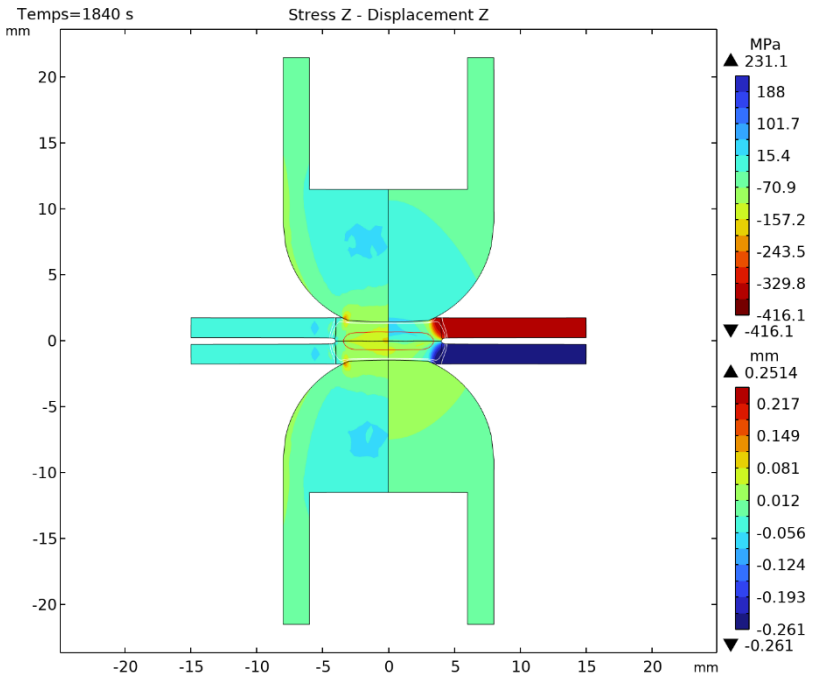

Fig. 4 Stress (left) and Displacement (right) along the z-axis for the ETMMHD model

Fig 5 shows the temperature field (on the left) and the velocity field within the molten zone (on the right), as computed by the model. In white, the contour represents the heat-affected zones (Ac1: 713 °C, Ac3: 825 °C), while the fusion contour delineating the molten zone is drawn in red. The magenta arrows indicate the flow directions of the molten pool. At first, we can observe the overall velocity field ranges is between 0 and 0.2 m/s, with isolated spikes along the axis of symmetry reaching up to 0.7 m/s. Although prior studies report molten-pool velocities between 0.3 and 0.6 m/s [4], the observed instabilities remain the subject of ongoing investigation. This behaviour is not unexpected, as asymmetric 2D models are inherently susceptible to anomalies along the symmetry axis.

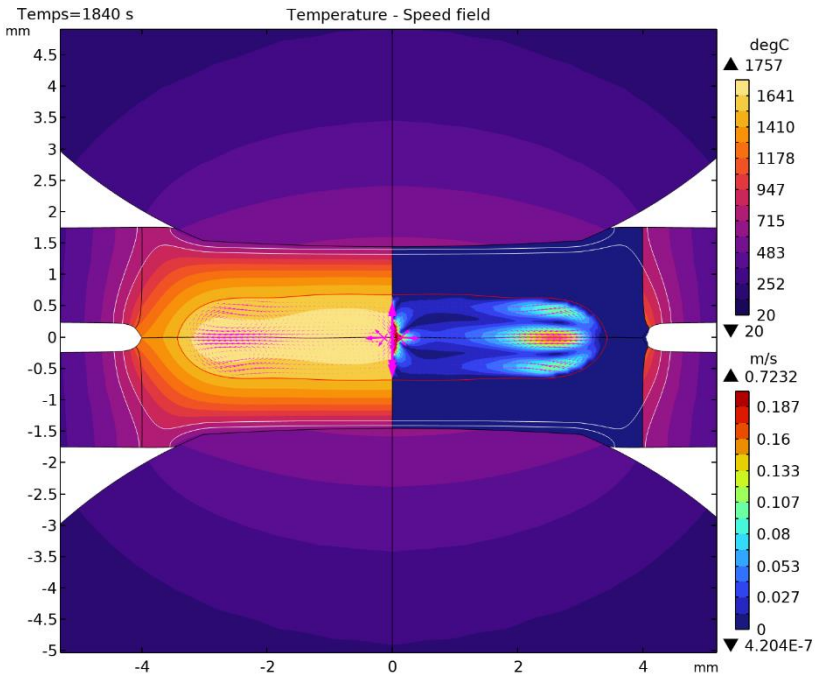

Fig. 5 Temperature and velocity fields in the molten pool (ETMMHD) at 340 ms (end the welding phase) for the ETMMHD model

In Fig 6, a very different temperature gradient can be observed, along with a different heat-affected zone. As previously mentioned, the integration of fluid flow into the model enables the representation of convection flows within the molten pool, leading to thermal homogenization that is not captured by conventional models (ETM), resulting in an overall inaccurate determination of the temperature field. As suggested in [2], the maximum expected temperature within the molten pool is approximately 1650 °C. However, Fig. 6 shows that the ETM model reaches a peak temperature of 2565 °C, which is significantly higher than that predicted by the ETMMHD approach (T_{max}= 1757 °C). This observation is consistent with the findings of [11], who reported notable differences between the thermal fields obtained using traditional electro-thermal and a magneto-hydro-dynamic models. Moreover, a notable difference appears in the shape of the molten zone, although it remains comparable in diameter to that obtained with the Electro-Thermo-Mechanical model alone.

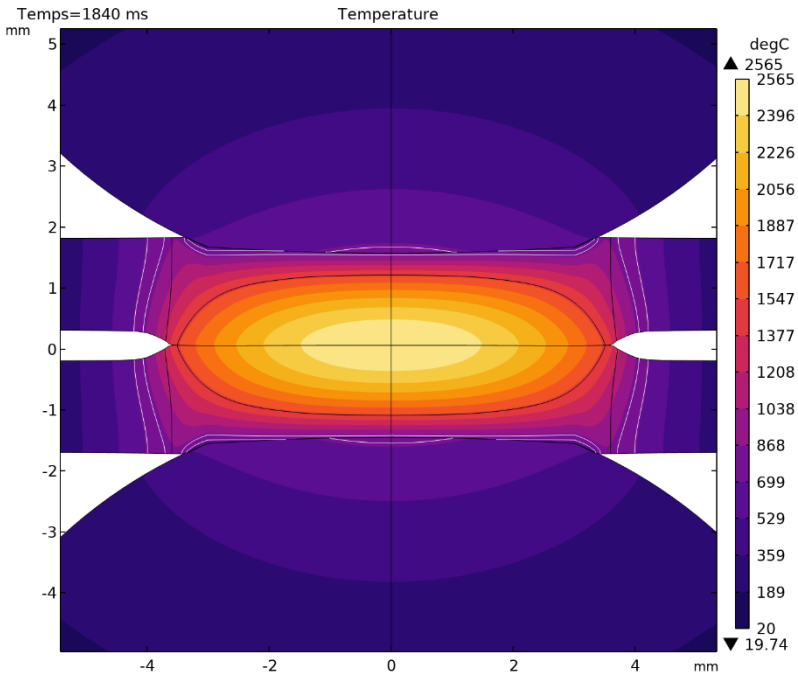

Fig. 6 Temperature field (Electro-Thermo-Mechanical Model) at 340 ms (end the welding phase)

Fig 7 presents a comparative graph of the molten zones and heat-affected zones (Ac1: 713 °C, Ac3: 825 °C) obtained for the two models. The Electro-Thermo-Mechanical model is shown in orange squares, while the ETMMHD model, integrating fluid flow and electromagnetism, is shown in purple triangles. As seen in Fig 5 and 6, there is a notable difference in the maximum temperature, with the ETMMHD model showing a reduction of approximately 825 °C. The addition of fluid flow allows for better thermal homogenization within the molten nugget. The detailed description of heat transfer within the molten pool influences areas beyond the liquid zone, with repercussions both on solid mechanics (through material properties) and on the understanding of the phenomenon under study, the interfacial expulsion.

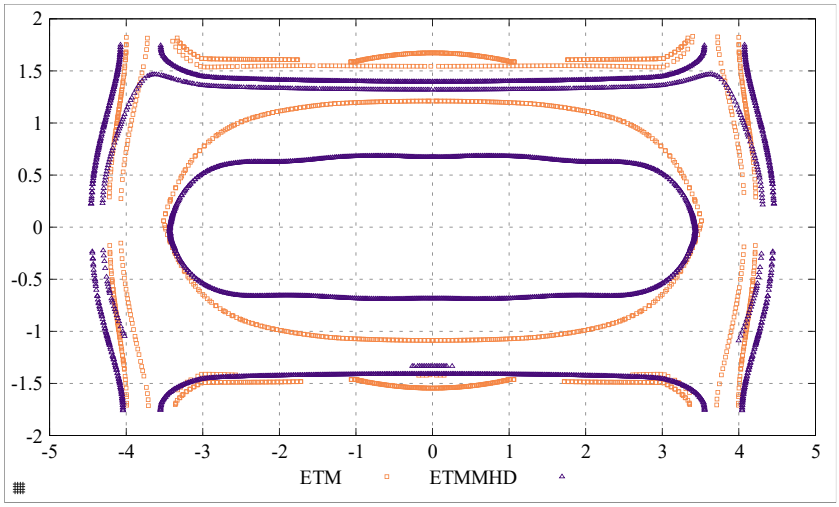

Fig. 7 Dimensions of the HAZ (Ac1 and Ac3 temperatures) and the MP for the two models (ETM: orange square – ETMMHD: purple triangle)

COMPARISON WITH EXPERIMENTAL DATA

To validate the numerical model, a comparison with experimental data was performed. The same welding parameters as those used in the simulation were applied, the only variation being the welding time, which ranged experimentally from 40 ms to 340 ms. This allowed us to observe the evolution of the molten pool during the welding process. Each configuration was repeated three times to ensure repeatability, and all dimensions were measured through macrographic cross-sections.

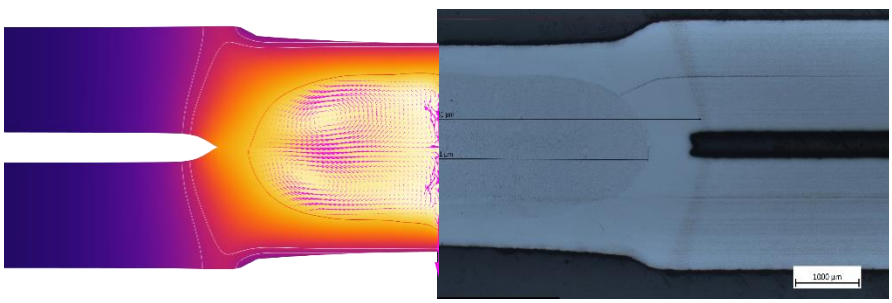

Fig. 8 Cross section comparison with the simulation

Fig 9 illustrates the evolution of the molten pool diameter during the welding phase. The ETM results are shown in orange (dashed line), the ETMMHD results in purple, and the

experimental data points are represented in red. Initially, both the ETM and ETMMHD models show an earlier onset of molten pool formation compared to the experimental results, with a lead of approximately 20 ms. Despite this time discrepancy, both models follow a similar trend and tend to overestimate the molten pool diameter during the welding phase. However, by the end of the welding phase, the predicted pool sizes from both models closely align with the experimental measurements.

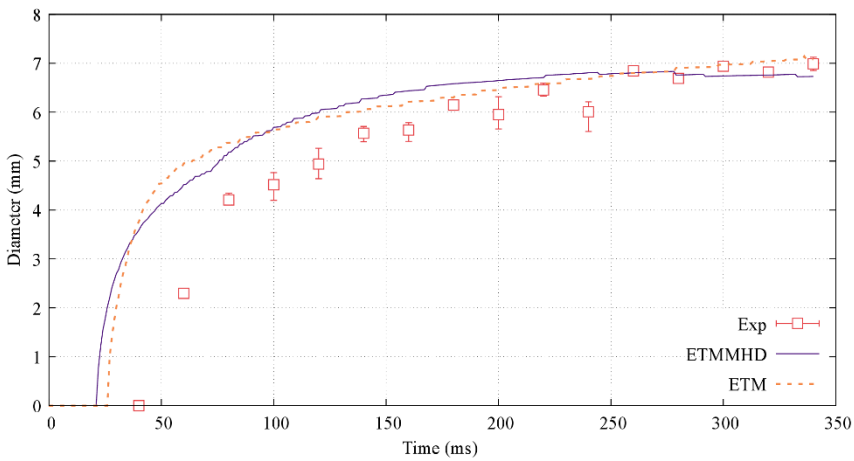

Fig. 9 Evolution of the molten pool diameter according to the ETM and ETMMHD models, and experimental data

Fig 10 shows the evolution of the molten pool thickness during the welding phase. Like the previous figure, both models predict an earlier appearance of the molten nugget compared to the experimental data. At the beginning of the process, the molten pool initially grows vertically, forming a thick nugget. As the indentation increases, the nugget becomes wider and thinner. The ETM model does not accurately capture this behaviour, as it continuously predicts an increasing nugget thickness. In contrast, the ETMMHD model, which incorporates a more realistic representation of convection within the nugget, shows a decrease in thickness over time like the experiment. Similar to the findings in [4], the results highlight the necessity of including fluid flow to accurately characterize the evolution of the melt-pool thickness. Although the ETMMHD model underestimates the nugget thickness throughout most of the process, it achieves a final molten pool thickness that matches the experimental result.

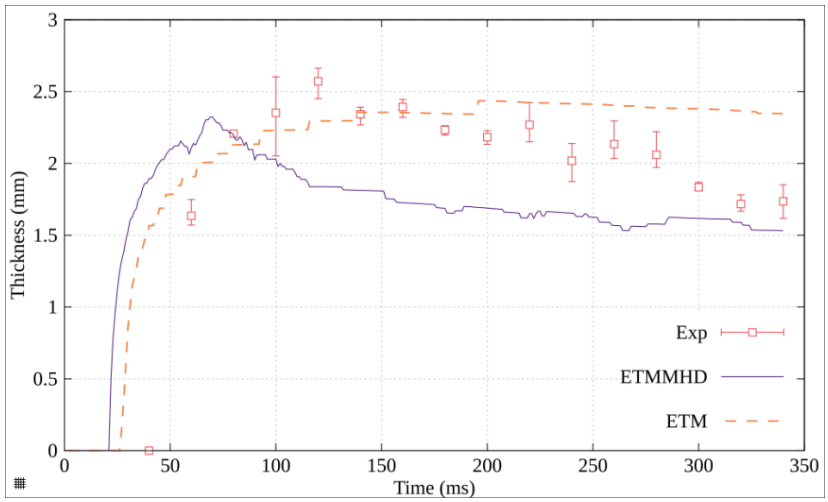

Fig. 10 Evolution of the molten pool thickness according to the ETM and ETMMHD models, and experimental data

CONCLUSION

This work presents a new simulation approach for the resistance spot welding (RSW) process, with the future goal of applying it to the study of the interfacial expulsion phenomenon. The developed model has demonstrated the feasibility of a strong, dynamic, and fully coupled interaction between electromagnetic, thermal, solid mechanical, and fluid flow phenomena using moving meshes (Arbitrary Lagrangian-Eulerian Formulation (ALE)). The key principle of using two separate meshes was introduced, allowing the model to overcome several constraints.

The initial results have highlighted the advantages of this approach, particularly through the improved representation of the temperature field, made possible by the explicit inclusion of molten pool flow, itself computed in geometry modified by solid mechanics. Comparison to both classical ETM model and experiments have shown the interest of the approach with satisfactory results. To our knowledge, this bidirectionally coupled approach solved at each time step has not yet been proposed in the literature for this type of process.

Building on this foundation, several improvements remain to be implemented. One priority involves refining contact conditions, particularly the adhesion models that represent the formation of the corona bond, which relates to the joining of material beyond the solid-state bonding temperature. Additionally, accounting for the thermal expansion coefficient of the fluid during the melting phase is another area for improvement, as this coefficient increases sharply during the solid-to-liquid transition.

Finally, an essential phase of a more thorough experimental validation of the model will be conducted, to assess the model's predictive capability and to fine-tune its parameters.

A final step in this project will be the transition to a 3D configuration, which would allow the consideration of directional aspects of expulsion and provide a more realistic representation of process imperfections, especially electrode misalignment.

References

[1] J. SENKARA, H. ZHANG and S. J. HU: 'Expulsion Prediction in Resistance Spot Welding', *Welding Journal – New-York,* vol. 83, No.4, pp 123-134, 2004.

[2] W. V. ALCINI: 'Experimental Measurement of Liquid Nugget Heat Convection in Spot Welding', *Welding Journal,* vol. 69, No.5, pp 177-180, 1990.

[3] Y. Li, Z. Luo, Y. Bai, et S. S. Ao: 'Investigation of induced magnetic force on liquid nugget during resistance spot welding', *Sci. Technol. Weld. Join.*, vol. 18, No 4, pp. 329-336, 2013.

[4] Y. B. LI, Z. Q. LIN, S. J. HU, ET G. L. CHEN: 'Numerical analysis of magnetic fluid dynamics behaviors during resistance spot welding', *J. Appl. Phys.*, vol. 101, No 5, pp. 101-109, 2007.

[5] D. J. BROWNE, H. W. CHANDLER, J. T. EVANS, P. S. JAMES, ET J. WEN: 'Computer Simulation of Resistance Spot Welding in Aluminum: Part II', *Welding Journal-Including Welding Research Supplement*, vol. 74, No 12, pp 417-422, 1995.

[6] Y. ZHANG, J. SHEN, ET X. LAI: 'Influence of Electrode Force on Weld Expulsion in Resistance Spot Welding of Dual Phase Steel with Initial Gap Using Simulation and Experimental Method', *ISIJ Int.*, vol. 52, No 3, pp 493-498, 2012.

[7] M. VALAEE-TALE, M. SHEIKHI, Y. MAZAHERI, F. MALEK GHAINI, ET G. R. USEFIFAR: 'Criterion for predicting expulsion in resistance spot welding of steel sheets', *J. Mater. Process. Technol.*, Vol. 275, pp. 116329, 2020.

[8] C. SRIKUNWONG: *Modélisation du procédé de soudage par points*, thesis, ENMP, Paris, France, 2005.

[9] R. RAOELISON: *Etude de l'influence des conditions interfaciales sur le développement du noyau lors du soudage par résistance par point*, thesis, Giens, France, 2011.

[10] COURTOIS, MICKAËL, CARIN, MURIEL, LE MASSON, PHILIPPE, ET GAIED, SADOK: 'Complete 3D heat and fluid flow modeling of keyhole laser welding and methods to reduce calculation times', *Math. Model. Weld Phenom.*, No.12, pp 1-11, Verlag der Technischen Universität Graz, 2018.

[11] Y. B. LI, Z. Q. LIN, S. J. HU, ET G. L. CHEN: 'Electromagnetic Phenomena in Resistance Spot Welding and its Effect on the Weld Nugget Formation', *Progress In Electromagnetics Research Symposium Proceedings*, Vol.3, pp 744-748, 2009.